

Agglomerates of aberrant DNA methylation are associated with toxicant-induced malignant transformation

Paul L. Severson,¹ Erik J. Tokar,² Lukas Vrba,^{3,4} Michael P. Waalkes² and Bernard W. Futscher^{1,3,*}

¹Department of Pharmacology and Toxicology; College of Pharmacy; University of Arizona; Tucson, AZ USA; ²National Toxicology Program Laboratory; National Institute of Environmental Health Sciences; Research Triangle Park, NC USA; ³University of Arizona Cancer Center; Tucson, AZ USA; ⁴Biology Centre ASCR; Institute of Plant Molecular Biology; Ceske Budejovice, Czech Republic

Keywords: epigenetics, arsenic, cadmium, DNA methylation, malignant transformation, long-range epigenetic silencing, agglomerative DNA methylation, H3K9me3, H3K27me3

Abbreviations: DMR, differentially methylated region; LRES, long-range epigenetic silencing; MeDIP, methyl-DNA immunoprecipitation; MDS, multidimensional scaling; H3K9me3, histone H3 lysine-9 trimethylation; H3K27me3, histone H3 lysine-27 trimethylation; MMA^{III}, monomethylarsonous acid; PCDH, protocadherin

Epigenetic dysfunction is a known contributor in carcinogenesis, and is emerging as a mechanism involved in toxicant-induced malignant transformation for environmental carcinogens such as arsenicals or cadmium. In addition to aberrant DNA methylation of single genes, another manifestation of epigenetic dysfunction in cancer is agglomerative DNA methylation, which can participate in long-range epigenetic silencing that targets many neighboring genes and has been shown to occur in several types of clinical cancers. Using in vitro model systems of toxicant-induced malignant transformation, we found hundreds of aberrant DNA methylation events that emerge during malignant transformation, some of which occur in an agglomerative fashion. In an arsenite-transformed prostate epithelial cell line, the protocadherin (PCDH), HOXC and HOXD gene family clusters are targeted for agglomerative DNA methylation. The agglomerative DNA methylation changes induced by arsenicals appear to be common and clinically relevant events, since they occur in other human cancer cell lines and models of malignant transformation, as well as clinical cancer specimens. Aberrant DNA methylation in general occurred more often within histone H3 lysine-27 trimethylation stem cell domains. We found a striking association between enrichment of histone H3 lysine-9 trimethylation stem cell domains and toxicant-induced agglomerative DNA methylation, suggesting these epigenetic modifications may become aberrantly linked during malignant transformation. In summary, we found an association between toxicant-induced malignant transformation and agglomerative DNA methylation, which lends further support to the hypothesis that epigenetic dysfunction plays an important role in toxicant-induced malignant transformation.

Introduction

Arsenic and cadmium are known carcinogens that are associated with many other chronic diseases; unsafe exposure levels to these toxicants remain a problem for millions of people throughout the world.^{1–4} Experiments have shown that long-term arsenic or cadmium exposure in vitro induces malignant transformation of several immortal cell lines, but the underlying mechanisms driving these toxicant-induced malignant transformations are multifaceted and remain elusive.^{5–8} Epigenetic dysfunction is emerging as an important aspect of both arsenic and cadmium associated chronic diseases, especially cancer.^{9–11}

In addition to genetic alterations, epigenetic changes are a driving force in cancer.¹² Earlier studies have shown that the aberrant DNA methylation profiles of distinct cancer models correlate

with the degrees of their aberrant phenotypes.^{13,14} In other words, as the phenotype of a cell progresses toward malignancy, its epigenetic patterning also becomes increasingly more distinct from that of its normal tissue counterpart. For example, during the immortalization of human mammary epithelial cells few to hundreds of differentially methylated regions (DMRs) arose concurrently and were correlated with the escape from distinct proliferation barriers.¹⁴ During the later stages of tumorigenic progression, DMRs were observed to accumulate more gradually while correlating with advanced malignant phenotypes.^{13,14}

In addition to targeting individual genes, cancer-associated epigenetic dysfunction is known to occur across large chromosomal regions which can encompass many genes. In normal cells, epigenetic mechanisms such as DNA methylation, histone H3 lysine-27 trimethylation (H3K27me3) and histone

*Correspondence to: Bernard W. Futscher; Email: bfutscher@azcc.arizona.edu
Submitted: 07/16/12; Revised: 09/06/12; Accepted: 09/10/12
<http://dx.doi.org/10.4161/epi.22163>

Table 1. Cell lines and samples analyzed by MeDIP-on-Chip

Sample	Exposure	Conc.	Duration	Culture post-exposure	Tumorigenic ^a	Reference
HUC (n = 2)	None	NA	NA	NA	ND	
UROtsa (n = 3)	None	NA	NA	NA	No	25, 55
URO-MSC12+24(-)	MMA ^{III}	50 nM	12 weeks	24 weeks	Yes	31
URO-MSC52	MMA ^{III}	50 nM	52 weeks	Yes	Yes	56
URO-ASSC	As ^{III}	1 μ M	52 weeks	Yes	Yes	5
URO-CDSC	Cd ^{II}	1 μ M	52 weeks	Yes	Yes	5
BFTC-905	As ^{III}	NA	NA	Yes	Yes	39
BFTC-909	As ^{III}	NA	NA	Yes	Yes	39
Bladder tumor (n = 6)	NA	NA	NA	NA	Yes	
PrEC (n = 2)	None	NA	NA	NA	ND	
RWPE-1 (n = 2)	None	NA	NA	NA	No	26
CAsE-PE (n = 2)	As ^{III}	5 μ M	33 weeks	None	Yes	6, 35
CTPE	Cd ^{II}	10 μ M	10 weeks	None	Yes	8, 57
WPE1-NB26	MNU	100 μ g/mL	4 cycles of 1 h	Yes	Yes	51
LNCaP	None	NA	NA	NA	Yes	58
PC3	None	NA	NA	NA	Yes	59
DU145	None	NA	NA	NA	Yes	60

NA, not applicable; ND, no data. ^aTumorigenic determination for the UROtsa and RWPE-1 cell lines including their derived counterparts is based on their ability to form tumors in immunocompromised mice. The remaining tumorigenic samples are listed as such because each was derived or isolated from a human tumor.

H3 lysine-9 trimethylation (H3K9me3) play important roles in silencing individual genes as well as large chromosomal regions or even entire chromosomes such as the inactive X of females (reviewed in ref. 15). Likewise, genomic scale analyses of cancers have shown that epigenetic dysfunction targets individual genes and larger chromosomal regions containing many genes.¹⁶⁻²⁰ These large scale aberrations of repressive epigenetic modifications have collectively been called long-range epigenetic silencing (LRES).²¹ Groups of DMRs that are enriched within defined chromosomal regions have been called agglomerative epigenetic aberrations and these agglomerative DNA methylation events can contribute to LRES.¹⁹ LRES events are unique epigenetic lesions that have been observed in various types of tumors, but they have not been linked to any specific carcinogen exposure.^{16,19,22-24} The fact that they are observed in tumors supports their clinical relevancy and suggests that carcinogen exposure could lead to their induction.

Our work examines two in vitro models, RWPE-1 and UROtsa, which have been used successfully to study epigenetic dysfunction associated with arsenical or cadmium-induced malignant transformation. These immortalized cell lines are non-tumorigenic and were derived from the prostate and ureter respectively, which are target sites for cadmium and arsenic-induced cancers.²⁵⁻³⁰ Long-term, independent exposures of these cell lines to arsenite (As^{III}), monomethylarsonous acid (MMA^{III}) and cadmium (Cd^{II}) induced hyperproliferation, conferred anchorage independent growth and tumorigenicity.^{5,6,8,31,32} The resulting tumorigenic cell lines provide valuable models to study the epigenetic component of arsenical or cadmium-induced malignant transformation in relevant target tissues. Previous

studies have shown that the arsenical or cadmium-transformed variants of RWPE-1 and UROtsa harbor stable aberrations to their DNA methylation profiles, including global hypomethylation and gene promoter hypermethylation.^{13,33-35}

We extend prior studies using higher resolution DNA methylation analyses, allowing us to gain further insights into aberrant DNA methylation patterns induced by long-term toxicant exposure. In this study we compare aberrant DNA methylation in two relevant models of arsenical or cadmium-induced malignant transformation, which enables us to distinguish the effects which are model-specific, toxicant-specific or generally found in cancers. Our results lend further support to the hypothesis that epigenetic dysfunction plays an important role in toxicant-induced malignant transformation by showing that clinically relevant, agglomerative aberrations of DNA methylation occur during arsenical and cadmium-induced malignant transformation.

Results

Malignant transformation by toxicants induces hundreds of DMRs in distinct models. This study was an effort to better understand the DNA methylation events of arsenic and cadmium-induced malignant transformation. Using MeDIP-on-Chip we analyzed the DNA methylation changes that occur during arsenical or cadmium-induced malignant transformation of immortal cell lines. **Table 1** lists the cell lines that were analyzed by MeDIP-on-Chip in this study with descriptions of their treatments and phenotypes. The schematic in **Figure 1A** shows the lineage of the in vitro models of toxicant target tissues used in this study which represent normal, immortal and malignant

phenotypes. HUC and PrEC are phenotypically normal cells with finite lifespans. Although these cell strains have distinct genotypes, their DNA methylation profiles can be used to represent that of the normal epithelial tissues of origin of UROtsa and RWPE-1 due to the stability and low variability of DNA methylation in normal tissues.^{36,37} We used this collection of normal, immortal and malignant models to help us put toxicant-induced aberrant DNA methylation into context with the methylation changes that occur generally in prostate and urothelial carcinogenesis.

To understand the context of the collective DNA methylation change associated with arsenical or cadmium-induced malignant transformation, we acquired a genome-wide DNA methylation profile for each of the cell lines and bladder tumors using MeDIPs coupled to 470,000 probe tiling human promoter microarrays that query 17,000 human gene promoters. We then used multidimensional scaling (MDS) to summarize the data from individual microarray probes and thus graphically represent the variability in the DNA methylation profiles between all the samples (Fig. 1B). The finite-lifespan cells, HUC and PrEC, are in close proximity to one another after MDS, which indicates that they have similar DNA methylation profiles. MDS also shows that the immortalized RWPE-1 and UROtsa cell lines do not cluster with the finite-lifespan cells, indicating that immortalization had a pronounced effect on the DNA methylation profiles of these cell lines, which is consistent with earlier studies that describe aberrant DNA methylation associated with immortalization.^{14,38} Of the two immortalized models, RWPE-1 has a methylation profile more similar to that of the finite-lifespan cells. In summary, the MDS shows that the normal cells have similar methylation profiles while the distinct immortalized cell lines have variable degrees of aberrant DNA methylation, which may be related to their pathways of immortalization.

Our analysis includes five cancer cell lines that collectively represent the

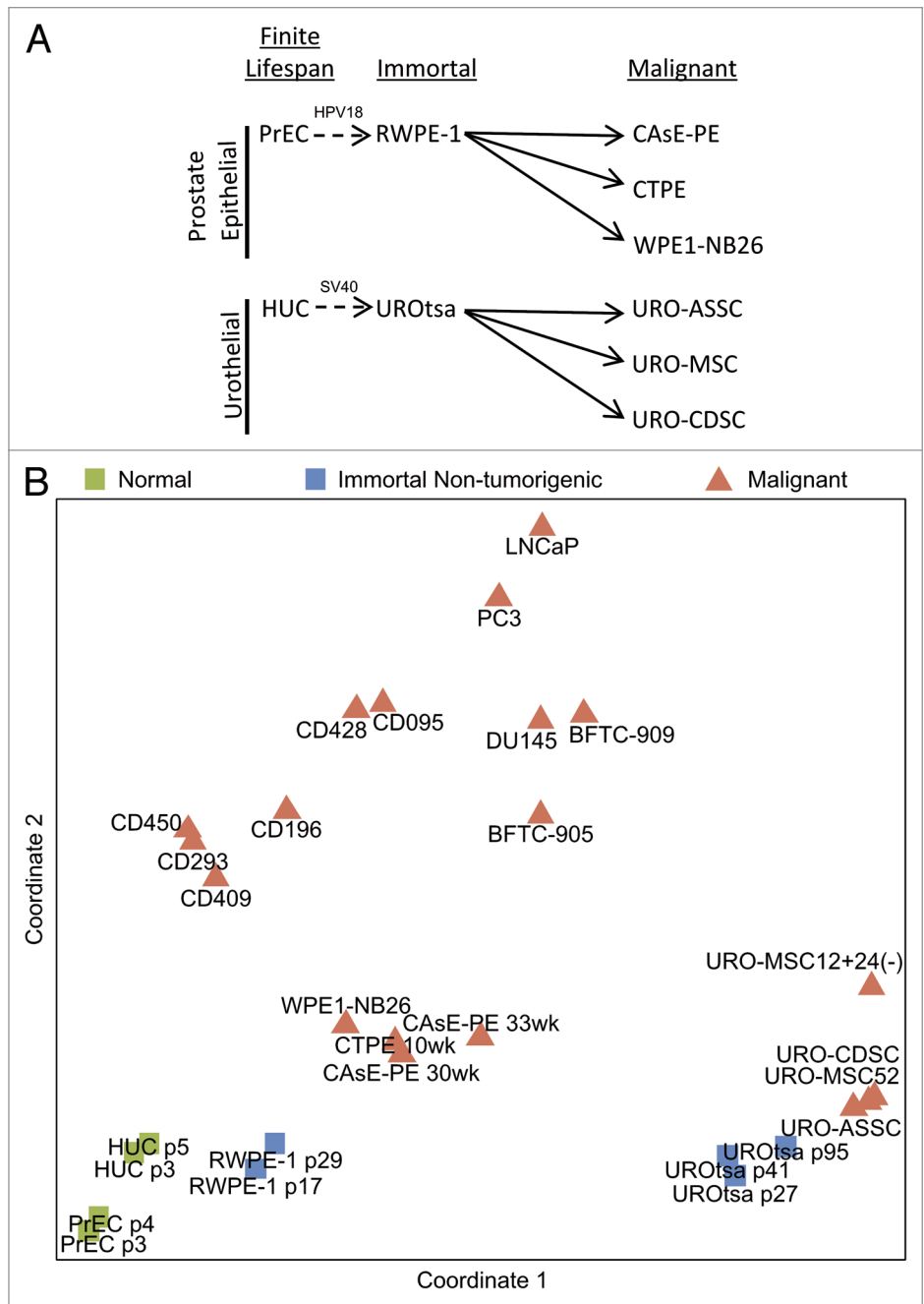


Figure 1. (A) Schematic showing the origins of the toxicant-transformed cell lines. The dashed arrows indicate that the finite-lifespan and immortal cells have distinct genotypes whereas the malignant cell lines are direct descendants of their corresponding immortal parent. The immortal RWPE-1 cell line was created from a primary culture of PrEC that was immortalized by the addition of HPV18. RWPE-1 cultures were chronically exposed to arsenite or cadmium to create the malignant cell lines CAsE-PE and CTPE. WPE1-NB26 cell were created by 100 μ g/mL MNU treatment. The immortal UROtsa cell line was created from a primary culture of HUC by the addition of an SV40 large-T antigen construct. UROtsa cells were malignantly transformed via long-term exposures to arsenite, MMA^{III} and cadmium giving rise to URO-ASSC, URO-MSc and URO-CDSC respectively. **(B)** Multidimensional scaling of pairwise distances derived from the DNA methylation level of gene promoters of all samples shows the relative similarity of the overall DNA methylation profiles of all the samples. The distances between samples in the MDS plot represent the degree of difference between the samples' methylation profiles. The six bladder tumor biopsies are labeled as CD450, CD409, CD293, CD196, CD095 and CD428. Arsenical or cadmium-induced malignant transformation of RWPE-1 alters the DNA methylation profile so that it more closely resembles the cancer cell lines and tumor biopsies.

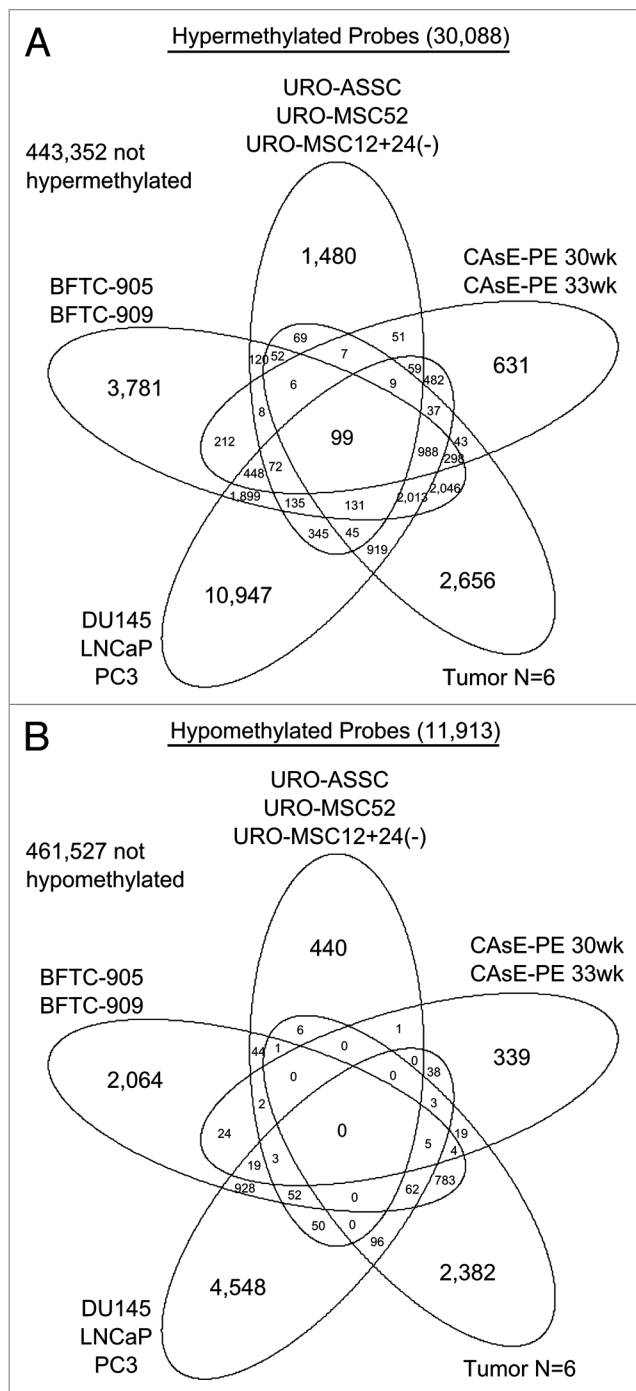


Figure 2. Venn Diagrams showing the numbers of significant probes compared with respective parent or normal that are shared between the different groups of malignant samples. **(A)** Hypermethylated probes commonly overlap between groups, which indicates that there are common targets of hypermethylation in the malignant samples. **(B)** There are fewer hypomethylated probes overall and they overlap less frequently which indicates that hypomethylation has fewer common targets between the malignant sample types.

aberrant DNA methylation events that occur in carcinogenesis. PC3, LNCaP and DU145 were each derived from metastatic prostate cancers and as such their methylation profiles reflect metastatic prostate cancer. The BFTC cell lines were derived from urothelial carcinomas of individuals who lived in Blackfoot disease endemic regions, which are regions specifically linked to high levels of environmental arsenic.³⁹ The prostate cancer cell lines and BFTC cell lines have the same tissue origins as RWPE-1 and UROtsa, and thus represent tissue matched models of the end stages of prostate and urothelial carcinogenesis. These five cancer cell lines are closer to one another than to the immortal or finite-lifespan cells in the MDS plot, which suggests that a portion of their DNA methylation profiles is common between them, but different from the other stages (e.g., finite-lifespan, immortal) (Fig. 1B). This is confirmed in Figure 2 which shows that the BFTC cell lines and the prostate cancer cell lines have a substantial overlap of differentially methylated probes compared with their respective finite-lifespan cells and 30% of these probes are not differentially methylated in immortalized cells compared with normal cells (Fig. S1).

In order to assure that the differences between the finite-lifespan cells and the cancer cell lines are relevant to clinical cancers, we included six human bladder tumor biopsies in our analysis. After MDS, the six tumors occupy a common region of the plot (Fig. 1B). This distribution of the tumor biopsies indicates that their DNA methylation profiles vary from one another while maintaining some similarity relative to the other sample types. Overall, the tumor biopsies are nearer to the cancer cell lines than to the finite lifespan cells which suggests that there may be a common set of aberrant DNA methylation events shared by both the clinical samples and cancer cell line models that correlates with their malignant phenotypes. Venn diagrams comparing aberrantly methylated probes between groups show that 26% of the differentially methylated probes in the tumor biopsy group are also differentially methylated in BFTC and prostate cancer cell lines, and 98% of these probes are hypermethylated (Fig. 2).

A comparison of the DNA methylation profiles of the virally-immortalized, non-tumorigenic cell lines RWPE-1 and UROtsa with their toxicant-transformed counterparts affords an estimate of the degree of aberrant DNA methylation induced by each toxicant. The MDS shows that in every case, transformation by toxicant exposure affected the DNA methylation profile in a similar way for each cell type. Each of the toxicant-transformed cell lines shifts in a similar direction relative to their untreated counterparts (Fig. 1B), which suggests that each has an analogous methylation change in a comparable portion of the probes. The DNA methylation changes that occur with toxicant-induced malignant transformation of RWPE-1 cells result in DNA methylation profiles that are more like cancer cell lines and tumor biopsies than before toxicant-induced transformation (Fig. 1B). The increasing similarity between DNA methylation profiles of toxicant-transformed RWPE-1 cells and those of cancer cell lines and tumor biopsies is driven mostly by hypermethylation since there are more hypermethylated probes and they overlap more often than hypomethylated probes (Fig. 2). Taken together, the MDS and Venn diagrams show that toxicants may induce

aberrant DNA methylation events that are common in cancer. In summary, an important interval of epigenetic change can be attributed to toxicant-induced transformation, and this interval correlates with the acquisition of a malignant phenotype.

To more finely resolve the epigenetic changes induced by toxicants and those associated with malignant transformation we identified specific DMRs between grouped samples. Compared with their parent cells, we found a total of 503 and 409 hyper DMRs in the CAsE-PE cells and arsenical-transformed UROtsa cells respectively (Fig. 3). Hypo DMRs were fewer, numbering 72 in CAsE-PE and 98 in the arsenical-transformed UROtsa lines. We also analyzed one cadmium-transformed variant of each immortal cell line as well as the WPE1-NB26 cells which showed that the number of cadmium or MNU-induced DMRs is comparable to those induced by arsenic. In summary, toxicant-induced malignant transformation causes hundreds of DMRs in distinct target tissues.

Agglomerates of aberrant DNA methylation in toxicant-transformed models. We next set out to locate extended regions of the genome that are enriched for DNA hypermethylation events after arsenical transformation of the RWPE-1 cells. This model was chosen to lead the study because the RWPE-1 cells had a relatively normal DNA methylation profile before exposure. In order to find agglomerative regions of aberrant DNA methylation we systematically scanned the MeDIP-on-Chip data by searching for genomic windows that contained more DMRs than expected by chance. Figure 4 shows in red the genomic locations where there is a significant enrichment of DMRs from the CAsE-PE cells. We found six genomic regions with significant enrichment of hyper DMRs in the CAsE-PE cells. These six genomic regions were further cropped to contain only runs of four or more DMRs with less than 200 kb between adjacent DMRs which left only three aberrant methylation events that meet these criteria (Table 2). These three agglomerative events target groups of consecutive genes in the protocadherin, HOXC and HOXD gene family clusters. The methylation status determined by MeDIP-on-Chip was confirmed for several of the DMRs within agglomerative regions using the MassARRAY EpiTYPER assay (Fig. 5; Figs. S2 and S3). The presence of these agglomerative events in the CAsE-PE cells indicates that arsenic-induced aberrant DNA methylation can target large chromosomal regions in addition to individual genes during malignant transformation.

Each of the three genomic regions with agglomerative hyper DMRs in CAsE-PE cells also shows aberrant hypermethylation in the BFTC cell lines, bladder tumor samples and prostate cancer cell lines relative to HUC or PrEC (Table 2). These regions are also hypermethylated after cadmium or MNU-induced transformations of RWPE-1 (Table 2, CTPe and WPE1-NB26). The commonality of hypermethylation in these regions suggests that they are not targets unique to arsenic-transformed cells, but are hypermethylated generally in prostate and urothelial cancers. The fact that some of the agglomerative DMRs are also observed in the bladder tumor biopsies, prostate cancer cell lines, black-foot cell lines, CTPe and WPE1-NB26 cells suggests that they are clinically relevant, bona fide epigenetic lesions that can be induced by exposure to multiple distinct toxicants (Figs. S4–8).

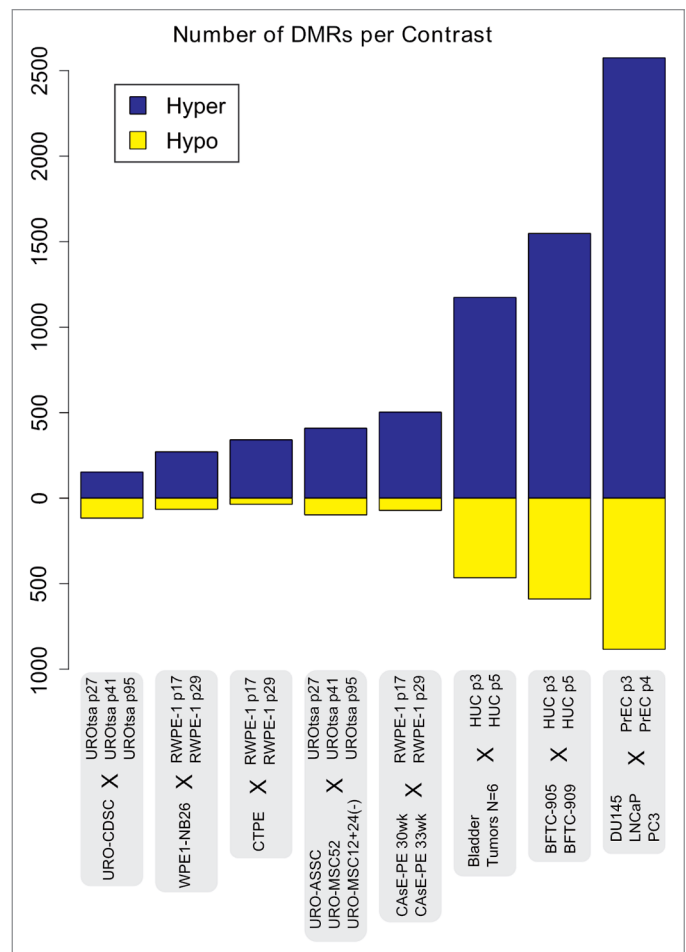


Figure 3. DMRs were calculated between the groups of samples shown. The blue and yellow bars show the number of hyper and hypo DMRs generated by the corresponding contrast.

The greatest enrichment of DNA hypermethylation in CAsE-PE cells occurred at the PCDH gene family cluster on chromosome 5 and at the HOXC gene family cluster on chromosome 12 (Fig. 4). The HOXC and PCDH gene family clusters are decisive examples of agglomerative, aberrant DNA methylation. The PCDH cluster has previously been identified in breast cancer as a target of agglomerative DNA hypermethylation and in Wilms' and colorectal tumors as a target of long-range epigenetic silencing.^{19,23,24} The HOXC clusters are also known targets of LRES,^{19,20} and specifically HOXC hypermethylation occurs in astrocytomas.⁴⁰

To better characterize the degree of aberrant methylation within the PCDH, HOXC and HOXD gene family clusters we hybridized independent MeDIPs of our samples to an additional Agilent tiling microarray of custom design. This array has extensive tiled coverage of all the HOX and PCDH gene family clusters giving more complete data with respect to the changing methylation pattern in these regions. On this custom array we found that in the CAsE-PE cells, the protocadherin G subfamily cluster (PCDHG) harbors 18 DMRs that collectively span 16 kb (Fig. 5). In the HOXC region there are 23 DMRs which

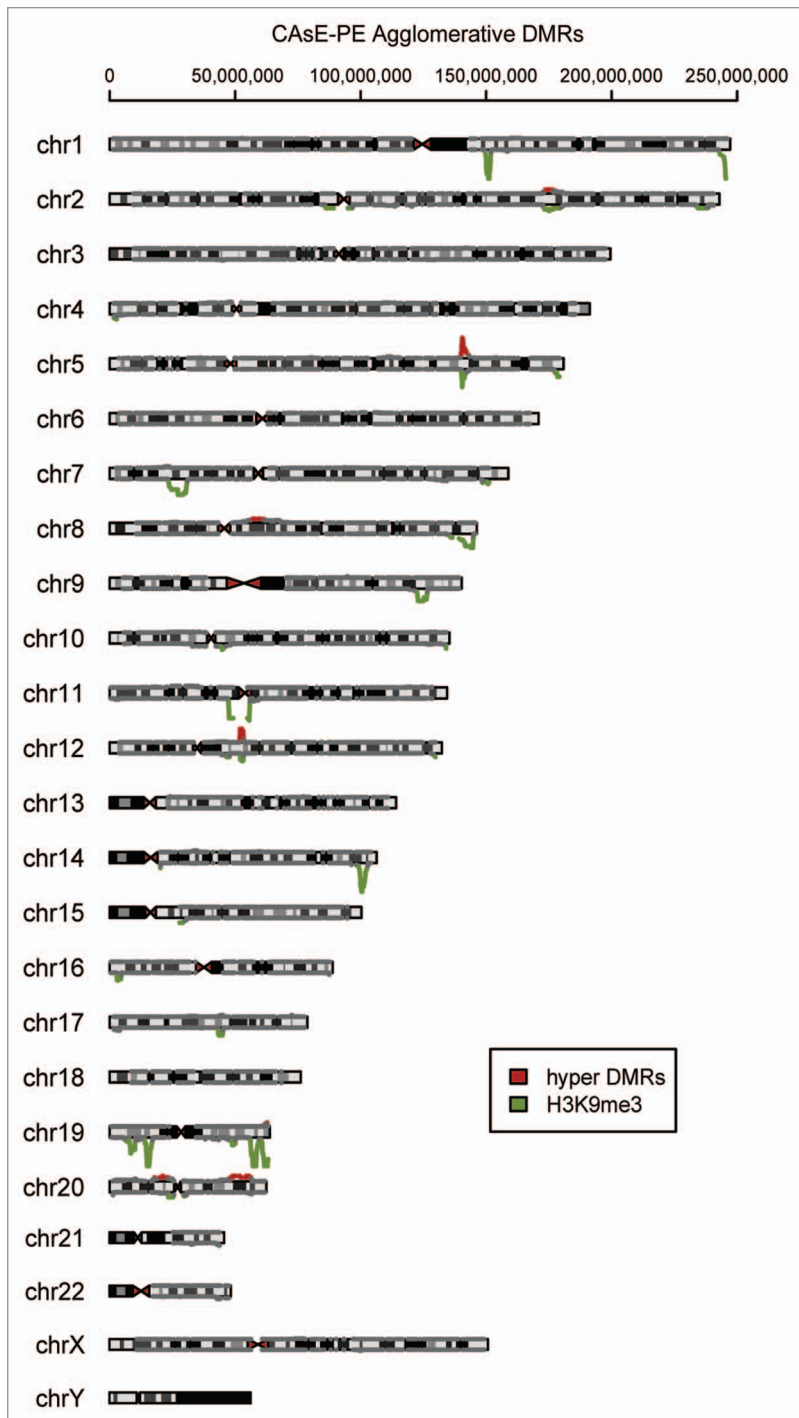


Figure 4. Hyper DMRs from CAsE-PE cells were analyzed for agglomerates. The negative \log_{10} of the p value calculated for each window was plotted as a distance from the respective chromosomal locations. The same calculation was applied to H3K9me3 stem cell domains to find regions of enrichment within the Agilent promoter ChIP-on-Chip microarray coverage. Points were plotted in red above or green below the corresponding chromosomal location when the enrichment of DMRs or H3K9me3 domains within the window was statistically significant (adjusted $p \leq 0.05$).

collectively span 28.4 kb of the 151 kb total array coverage in this region (Fig. S2). Within these regions, there is at least one DMR for nearly every gene promoter and these DMRs associate

with the CpG islands of the promoters. The HOXD region contains only five DMRs (Fig. S3).

Association of arsenical-induced agglomerative DMRs with histone modification domains of embryonic stem cells. In order to better understand the potential mechanisms of arsenic-induced epigenetic dysfunction, we compared the DMRs found in CAsE-PE cells with known domains of histone modifications in human embryonic stem cells. H3K27me3 and H3K9me3 domains of stem cells were determined previously.⁴¹ H3K27me3 is a transcriptionally repressive mark deposited by the polycomb group proteins and genes that are polycomb targets in stem cells are often targets of aberrant DNA methylation in tumors.^{42,43} H3K9me3 is also a repressive mark and an important component of heterochromatin which has been shown to work in concert with DNA methylation in part by directing its spreading.⁴⁴⁻⁴⁶ Comparing the locations of DMRs to H3K27me3 and H3K9me3 stem cell domains may help determine if aberrant DNA methylation is linked to either of these histone modifications.

To assess the spatial relationships between the arsenical-induced hypermethylation and the stem cell histone modification domains we calculated the number of hypermethylated microarray probes from CAsE-PE cells that occur within H3K27me3 or H3K9me3 stem cell domains. **Figure 6** shows that 76 and 18 percent of the hypermethylated probes in CAsE-PE cells overlap H3K27me3 and H3K9me3 stem cell domains, respectively. These overlaps are highly significant based on the expected overlaps of 27 and four percent for H3K27me3 and H3K9me3 domains, respectively. These results suggest that H3K27me3 and H3K9me3 stem cell domains are susceptible to aberrant DNA methylation during malignant transformation of CAsE-PE cells.

Next we assessed whether the CAsE-PE agglomerative DNA methylation events associate with genomic regions enriched with H3K27me3 or H3K9me3 stem cell domains. To do this we scanned the portion of the genome covered by the human promoter microarray for extended regions that were enriched with these domains and compared them to the locations of the agglomerative DMRs. Enriched regions of H3K27me3 domains partially overlapped the CAsE-PE agglomerative events in an expected manner considering that H3K27me3 stem cell domains cover almost 27 percent of the microarray. There was a striking overlap of the H3K9me3 enriched regions with the agglomerative DNA methylation events. **Figure 4** shows in green the genomic locations where there is a significant enrichment of H3K9me3 stem cell domains. In the CAsE-PE cells, all three of the agglomerative DNA methylation events overlap with significant peaks of H3K9me3 domain enrichment

Table 2. Genomic regions of arsenic-induced agglomerative DNA hypermethylation in CAsE-PE cells (n = 2) found with the Agilent promoter ChIP-on-Chip microarray

Chr	From (bp)	To (bp)	Size (kbp)	# of DMRs	Genes with DMRs	Other groups or samples with hypermethylation
chr 2	176678716	176760984	82	5	HOXD11, HOXD10, HOXD3, HOXD1	(LNCaP, PC3 and DU145), CTPE, (bladder tumors), [URO-ASSC, URO-MSC12+24(-) and URO-MSC52], URO-CDSC, (BFTC-905 and BFTC-909), WPE1-NB26
chr 5	139907571	140844320	937	18	EIF4EBP3, CD14, PCDHA3, PCDHAC2, PCDHB6, PCDHB7, PCDHB16, PCDHGA2, PCDHGA3, PCDHGB4, PCDHGA8, PCDHGB5, PCDHGA10, PCDHGB7, PCDHGA11, PCDHGA12, PCDHGC4	(LNCaP, PC3 and DU145), CTPE, (bladder tumors), (BFTC-905 and BFTC-909), WPE1-NB26
chr 12	52616802	52732432	116	15	HOXC13, HOXC12, HOXC11, HOXC10, hsa-mir-196a2, HOXC9, HOXC8, HOXC6, HOXC5, HOXC4	(LNCaP, PC3 and DU145), CTPE, (bladder tumors), [URO-ASSC, URO-MSC12+24(-) and URO-MSC52], URO-CDSC, (BFTC-905 and BFTC-909), WPE1-NB26

Consecutive genomic windows with $p \leq 0.05$ (Fig. 4) were trimmed to include only the regions that contain runs of 4 or more DMRs with less than 200 kb between adjacent DMRs. This filter was based on randomized CAsE-PE hyper DMR data, which showed that the expected number of runs with four or more DMRs and 200 kb or less between them is zero. In the non-randomized CAsE-PE data there are three runs that meet these criteria and occur within significant windows of hyper DMR enrichment. Other samples with hyper DMRs in these regions are shown in the final column. Samples in parenthesis were analyzed as groups.

(Fig. 4). These occur at the HOXD cluster on chromosome 2, the PCDH cluster on chromosome 5 and the HOXC cluster on chromosome 12. These overlaps suggest a potential connection between H3K9me3 stem cell domains and agglomerative DNA methylation.

Discussion

This study reports agglomerative DNA hypermethylation in toxicant-transformed cell lines, linking chronic arsenic and cadmium exposures in vitro with hypermethylation of large chromosomal regions. This new association supports the hypothesis that epigenetic dysfunction plays an important role in arsenic-induced malignant transformation because the agglomerative events are clinically relevant, occurring in human tumor samples (Fig. S5). Agglomerative DNA hypermethylation is one modification that is sometimes involved in LRES.¹⁸⁻²⁰ LRES events have been observed in various human tumors and they reduce the transcriptional plasticity of groups of consecutive genes.⁴⁷ While our study does not specifically address transcriptional silencing caused by these arsenic-induced agglomerative events, it does identify regions that are known sites of LRES in other models.^{19,20,23,24} We suspect that agglomerative DNA methylation often occurs at genes whose expression is already repressed by some other mechanism. Based on this study, we propose that while the agglomerative DNA methylation events are not always driving gene expression changes, they may represent deep epigenomic scars left by malignancy driving catastrophic events caused by toxicant exposure.

The agglomerative DNA hypermethylation events that occur at the PCDH and HOXC clusters were independently induced during arsenite, cadmium and MNU mediated malignant

transformations, suggesting that they are reproducible events (Fig. 4; Figs. S4 and S8). Therefore, the RWPE-1/CAsE-PE cell line model can be used as a tractable system in which to study the mechanisms involved in agglomerative DNA methylation and LRES, especially in the candidate regions found here such as the HOX and PCDH gene family clusters. The reproducibility of these events by distinct toxicants also suggests that each perturbs some common pathways involved in epigenetic dysfunction. Such a pathway could be related to the strong associations found between the H3K27me3 and H3K9me3 stem cell domains and aberrant DNA methylation. In general, there appear to be genomic locations which are highly susceptible to aberrant DNA methylation during toxicant-mediated malignant transformation.

In the arsenical-transformed UROtsa models we observed only one potential region of agglomerative DMRs (Fig. S9), which occurs at the HOXB gene family cluster. The lack of agglomerative DNA methylation events in the arsenical-transformed UROtsa cells relative to CAsE-PE appears related to the epigenetic state of the parental UROtsa prior to arsenic exposure. The pathway of events that gave rise to the immortal UROtsa cell line induced pronounced epigenetic remodeling. This is apparent in the comparison of UROtsa with HUC, which shows many agglomerative DNA methylation events are present in the UROtsa cells prior to any arsenic exposure (Fig. S10). This finding is not unprecedented since others have also observed agglomerative DNA methylation associated with catastrophic events such as overcoming stasis or immortalization.¹⁴ This can help explain why arsenic did not induce as many agglomerative events in the arsenical-transformed UROtsa models compared with CAsE-PE, because genomic regions likely targeted for agglomerative DNA methylation during arsenic exposure were already

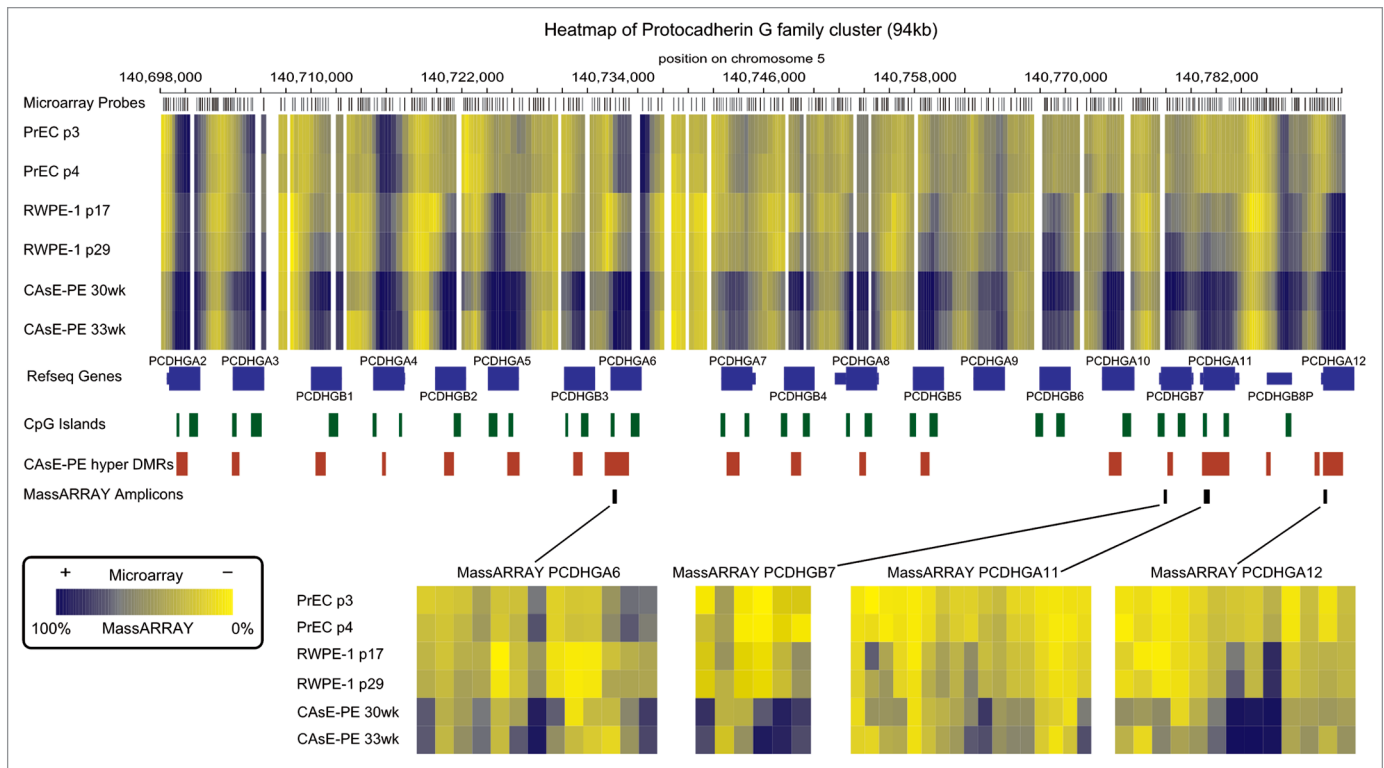


Figure 5. Protocadherin G gene family cluster heatmap generated from the custom Agilent tiling MeDIP-on-Chip microarray data. The color of each tile in the heatmap represents the relative degree of methylation. Refseq genes, CpG islands and CAsE-PE ($n = 2$) hyper DMRs are shown below the heatmap in their corresponding locations. The small black bars mark the regions that were confirmed by the MassARRAY EpiTYPER assay. The smaller heatmaps were generated from the MassARRAY EpiTYPER data and the coloring of each tile represents the degree of methylation of each CpG unit from 0% to 100%.

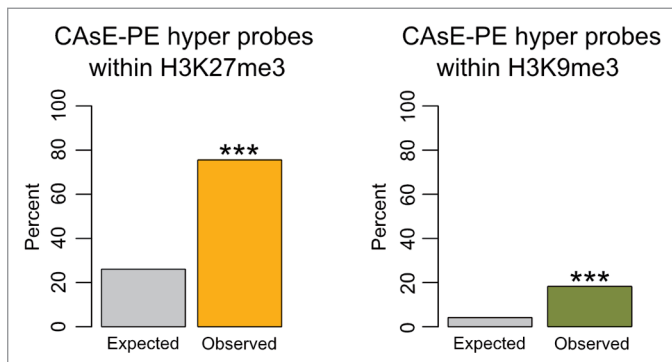


Figure 6. Total number of hypermethylated probes from CAsE-PE ($n = 2$) that fall within H3K27me3 or H3K9me3 stem cell domains. 76% of the hypermethylated probes are within H3K27me3 domains (orange) when only 27% were expected. Eighteen percent of the hypermethylated probes are within H3K9me3 domains (green) when only 4% are expected (***) $p \leq 1 \times 10^{-16}$, hypergeometric test).

hypermethylated in the parental UROtsa. These observations also highlight RWPE-1 as a valuable model to study the epigenetic mechanisms of toxicant-induced malignant transformation because its DNA methylation profile is relatively normal despite being an immortalized cell line.

Several important similarities and connections exist between stem cells and cancer cells that support an epigenetic comparison of these distinct cell types (reviewed in ref. 48). First, both exhibit self-renewal capability. Second, cancer cells often lose the terminally differentiated phenotype of their normal tissue counterparts to resemble undifferentiated or stem cells. Finally, all normal differentiated cells and cancer cells are descendants of stem cells. These similarities and observations provide rationale for a comparison of the distinct epigenetic states between normal embryonic stem cells and our malignantly transformed models and suggest that the epigenetic state of malignant cells could be related to or partially determined by that of their stem cell ancestors.

As expected, we found that H3K27me3 stem cell domains significantly overlapped individual hyper DMRs that arise during toxicant-induced malignant transformation (Fig. 6). An association between H3K27me3 domains and aberrant DNA methylation in cancer has been described previously, which lends support to our data analysis because it conforms with the findings of several other studies.^{40,42,43} When we compared the enrichment of H3K27me3 and H3K9me3 domains to CAsE-PE agglomerative DNA methylation only the H3K9me3 enriched regions had a striking overlap with the agglomerative DMRs (Fig. 4). This supports the link between H3K27me3 and aberrant hypermethylation of individual genes, but in the case of

agglomerative hypermethylation, H3K9me3 may be a more important player.

The significant overlaps observed between stem cell H3K9me3 enriched domains and the toxicant-induced agglomerative DMRs suggest that H3K9me3 modifications may be involved in directing aberrant DNA methylation to these regions. While the association of aberrant DNA methylation with H3K9me3 in humans is rather new, normal mechanisms are known which link these two epigenetic modifications. For example, both are hallmarks of normal mammalian heterochromatin and the histone methyltransferases Suv39h and G9a have been shown to recruit DNA methyltransferases which can lead to spreading of DNA methylation in normal cells.⁴⁴⁻⁴⁶ On the other hand, there must also be normal mechanisms leading to H3K9me3 that do not induce DNA methylation since many H3K9me3 domains in normal cells are not DNA methylated.⁴⁹ Perhaps during malignant transformation there are aberrant interactions between histone methyltransferases and DNA methyltransferases (e.g., Suv39h and DNMT3B) that lead to aberrant DNA methylation of H3K9me3 domains that are normally unmethylated. Once such a region contains aberrant DNA methylation, H3K9me3 and its associated factors may induce further spreading of the aberrant methylation to result in an agglomerative region of aberrant DNA methylation.^{45,46}

In conclusion, agglomerative DNA methylation is associated with toxicant-induced malignant transformation. Overall, this study suggests that there are common pathways of epigenetic dysfunction in distinct models transformed by arsenic, cadmium or MNU, which target both individual genes as well as larger chromosomal regions that contain many genes. Individual DMRs are likely to occur in H3K27me3 domains while the agglomerative DNA methylation may be targeted to H3K9me3 domains. These associations provide further insights into the epigenetic mechanisms of toxicant-induced malignant transformation and carcinogenesis in general.

Materials and Methods

Cell culture and sample acquisition. UROtsa, URO-ASSC and URO-CDSC cells were contributed by Drs Donald and Mary Ann Sens. The UROtsa cell line was created from the urothelial cells of a 12-y-old female donor that were immortalized using a temperature sensitive SV40 large-T antigen construct.²⁵ URO-ASSC cells were created through continuous exposure of UROtsa to 1 μ M arsenite for one year.⁵ Similar to the arsenite-induced transformation, URO-CDSC cells were created by continuous exposure of UROtsa to 1 μ M cadmium for one year.⁵ URO-MSC cell lines were contributed by Dr Jay Gandolfi and were created through continuous exposure of UROtsa cells to 50 nM MMA^{III} as previously described.³¹ Each of the UROtsa cell lines was cultured as previously described.³⁴ The blackfoot transitional cell carcinoma lines (BFTC-905 and BFTC-909) were acquired from the German Collection of Microorganisms and Cell Cultures.^{39,50} BFTC-905 and BFTC-909 were derived from urothelial carcinomas of individuals who lived in blackfoot endemic regions of Taiwan where high level exposure to

arsenic is common. BFTC-905 and BFTC-909 were cultured at 37°C with 5% CO₂ in DMEM with 10% FBS and 1% vol/vol penicillin-streptomycin solution with media changes three times per week and sub-culturing before reaching confluence. The non-tumorigenic RWPE-1 cell line was derived from prostate epithelial cells that were infected with human papillomavirus 18 to induce immortalization.²⁶ RWPE-1 cells were cultured in K-SFM with 50 μ g/mL BPE, 5 ng/mL EGF, and 1% vol/vol antibiotic-antimycotic solution. RWPE-1 cells were continuously exposed to 5 μ M sodium arsenite for up to 33 weeks and are referred to as CAsE-PE cells after undergoing arsenite-induced malignant transformation.^{6,35} RWPE-1 cells were also malignantly transformed by exposure to 10 μ M cadmium for 10 weeks and the resulting line is called cadmium-transformed prostate epithelial cells (CTPE). WPE1-NB26 is a malignant cell line that was created previously by exposure of RWPE-1 cells to 100 μ g/mL N-methyl-N-nitrosourea (MNU) for 4 cycles of 1 h/passage, after which cells were selected by xenografting twice through nude mice and growth on soft agar.⁵¹ WPE1-NB26 cells were cultured as previously described.⁵¹ Normal human prostate epithelial cells (PrEC) cryopreserved at passage two were acquired from ATCC and cultured in PrEBMTM with added BulletKitTM (Lonza). Normal female human urothelial cells (HUC) were acquired from ScienCellTM Research Laboratories and cultured in Urothelial Cell Medium (ScienCell Research Laboratories). The prostate cancer cell lines PC3, LNCaP and DU145 were cultured in Iscove's Modified Dulbecco's Medium (IMDM), RMPI-1640 and IMDM respectively with 10% FBS and 1% vol/vol antibiotic-antimycotic solution at 37°C and 5% CO₂. Short tandem repeat (STR) profiling was performed on each cell line either to validate its origin or confirm a unique DNA profile in the case where none has been published. DNA samples from six human urothelial carcinoma tumor biopsies were purchased from Origene Technologies.

Nucleic acid isolation. Genomic DNA was isolated using the DNeasy Blood and Tissue Kit according to manufacturer's protocol (Qiagen). The quantity of each sample was assessed using absorbance at 260 nm on the NanoDrop 1000 Spectrophotometer.

MeDIP coupled to microarray (MeDIP-on-Chip). MeDIPs were performed as previously described.⁵² MeDIP and input samples were amplified, labeled, hybridized and washed as previously described.⁵³ The following modifications were made for samples hybridized to the G4489A Human Promoter ChIP-on-Chip Microarray Set 244K designs 014706 and 014707 (Agilent Technologies). Two micrograms of each amplified MeDIP and input were labeled for each slide of the 2-slide set. After labeling, the MeDIPs and inputs were combined and then divided into two equal volumes before drying down to 187.5 μ L each. To each was added 12.5 μ L human cot-1 DNA (1 mg/mL, Invitrogen Cat. No. 15279-011), 50 μ L 10 \times Agilent blocking agent and 250 μ L 2 \times Agilent hybridization buffer before incubation at 95°C, 37°C and hybridization. Independent MeDIPs and inputs from identical or similar samples to those used on the Agilent G4489A Human Promoter ChIP-on-Chip Microarray Set 244K were amplified, labeled and hybridized to a custom Agilent tiling

microarray, design 024305, as previously described.⁵³ This microarray covers 718 miRNA hairpin regions and includes extensive tiled coverage of all the HOX and protocadherin gene family clusters.

MeDIP-on-Chip data analysis. Microarray data were imported to R⁵⁴ and normalized as previously described.⁵³ M values (log₂ ratios of immunoprecipitated and input channel) were used for further analysis as a measure of enrichment of a region centered on individual probes. The multidimensional scaling plot was generated using pairwise distances between samples that were derived from all M values and the function `cmdscale` in R. For calculation of DMRs, M values were analyzed in a sliding window of 1,200 bp, with a step of one probe. DMRs were defined as regions of at least three consecutive probes less than 600 bp apart where the mean difference of ratios was at least 1.5 fold. A p value cut was selected to maintain the false discovery rate (FDR) ≤ 1%. The FDR was determined by analysis of permuted data.

Detection of agglomerates and regions enriched with stem cell domains. The Agilent G4489A promoter microarray coverage was binned and annotated to individual genes. Each annotated bin was considered positive if it overlapped the domain of interest (DMR, H3K27me₃ or H3K9me₃ stem cell domain). Data were analyzed in windows of 49 consecutive bins with a step of one bin using the hypergeometric test for the difference of the expected and observed number of positive bins in each window. P values were adjusted for multiple testing.

MassARRAY EpiTYPER™ DNA methylation analysis. EpiTYPER DNA methylation analysis was performed as previously described (Sequenom).^{14,19} The EpiTYPER primer

sequences and amplicon locations are provided (Fig. 5; Table S1 and Figs. S2 and 3).

Data access. Microarray data were deposited in NCBI's Gene Expression Omnibus (GEO) (www.ncbi.nlm.nih.gov/geo) under accession number GSE38930.

Disclosure of Potential Conflicts of Interest

No potential conflicts of interest were disclosed.

Acknowledgments

This work was supported by the National Institutes of Health (P42 ES04940, ES006694, CA23074, 5T32ES16652-3 to P.S.). We thank the laboratory of Dr A. Jay Gandolfi for providing the URO-MS52 and URO-MS12+24(-) cell lines. We are grateful to the laboratory of Drs Donald and Mary Ann Sens for sharing UROtsa, URO-ASSC and URO-CDSC. We wish to thank Dr Petr Novak for contributing his time and insightful comments. The costs for publication of this article were deferred by the Southwest Environmental Health Sciences Center (ES006694). This article may be the work product of an employee or group of employees of the National Institute of Environmental Health Sciences (NIEHS), National Institutes of Health (NIH), however, the statements, opinions or conclusions contained therein do not necessarily represent the statements, opinions or conclusions of NIEHS, NIH or the US government.

Supplemental Materials

Supplemental materials may be found here: www.landesbioscience.com/journals/epigenetics/article/22163

References

1. IARC Working Group on the Evaluation of Carcinogenic Risks to Humans. Some drinking-water disinfectants and contaminants, including arsenic. IARC Monogr Eval Carcinog Risks Hum 2004; 84:1-477; PMID:15645577.
2. Chen Y, Graziano JH, Parvez F, Liu M, Slavkovich V, Kalra T, et al. Arsenic exposure from drinking water and mortality from cardiovascular disease in Bangladesh: prospective cohort study. *BMJ* 2011; 342:d2431; PMID:21546419; <http://dx.doi.org/10.1136/bmj.d2431>.
3. Vahter M. Health effects of early life exposure to arsenic. *Basic Clin Pharmacol Toxicol* 2008; 102:204-11; PMID:18226075; <http://dx.doi.org/10.1111/j.1742-7843.2007.00168.x>.
4. Huff J, Lunn RM, Waalkes MP, Tomatis L, Infante PF. Cadmium-induced cancers in animals and in humans. *Int J Occup Environ Health* 2007; 13:202-12; PMID:17718178.
5. Sens DA, Park S, Gurel V, Sens MA, Garrett SH, Somji S. Inorganic cadmium- and arsenite-induced malignant transformation of human bladder urothelial cells. *Toxicol Sci* 2004; 79:56-63; PMID:14976345; <http://dx.doi.org/10.1093/toxsci/kfh086>.
6. Achanzar WE, Brambila EM, Diwan BA, Webber MM, Waalkes MP. Inorganic arsenite-induced malignant transformation of human prostate epithelial cells. *J Natl Cancer Inst* 2002; 94:1888-91; PMID:12488483; <http://dx.doi.org/10.1093/jnci/94.24.1888>.
7. Wang Z, Zhao Y, Smith E, Goodall GJ, Drew PA, Brabletz T, et al. Reversal and prevention of arsenic-induced human bronchial epithelial cell malignant transformation by microRNA-200b. *Toxicol Sci* 2011; 121:110-22; PMID:21292642; <http://dx.doi.org/10.1093/toxsci/kfr029>.
8. Achanzar WE, Diwan BA, Liu J, Quader ST, Webber MM, Waalkes MP. Cadmium-induced malignant transformation of human prostate epithelial cells. *Cancer Res* 2001; 61:455-8; PMID:11212230.
9. Ren X, McHale CM, Skibola CF, Smith AH, Smith MT, Zhang L. An emerging role for epigenetic dysregulation in arsenic toxicity and carcinogenesis. *Environ Health Perspect* 2011; 119:11-9; PMID:20682481; <http://dx.doi.org/10.1289/ehp.1002114>.
10. Hou L, Zhang X, Wang D, Baccarelli A. Environmental chemical exposures and human epigenetics. *Int J Epidemiol* 2012; 41:79-105; PMID:22253299; <http://dx.doi.org/10.1093/ije/dyr154>.
11. Bollati V, Baccarelli A. Environmental epigenetics. *Heredity (Edinb)* 2010; 105:105-12; PMID:20179736; <http://dx.doi.org/10.1038/hdy.2010.2>.
12. Sharma S, Kelly TK, Jones PA. Epigenetics in cancer. *Carcinogenesis* 2010; 31:27-36; PMID:19752007; <http://dx.doi.org/10.1093/carcin/bgp220>.
13. Jensen TJ, Novak P, Wnek SM, Gandolfi AJ, Futscher BW. Arsenicals produce stable progressive changes in DNA methylation patterns that are linked to malignant transformation of immortalized urothelial cells. *Toxicol Appl Pharmacol* 2009; 241:221-9; PMID:19716837; <http://dx.doi.org/10.1016/j.taap.2009.08.019>.
14. Novak P, Jensen TJ, Garbe JC, Stampfer MR, Futscher BW. Stepwise DNA methylation changes are linked to escape from defined proliferation barriers and mammary epithelial cell immortalization. *Cancer Res* 2009; 69:5251-8; PMID:19509227; <http://dx.doi.org/10.1158/0008-5472.CAN-08-4977>.
15. Trojer P, Reinberg D. Facultative heterochromatin: is there a distinctive molecular signature? *Mol Cell* 2007; 28:1-13; PMID:17936700; <http://dx.doi.org/10.1016/j.molcel.2007.09.011>.
16. Frigola J, Song J, Stirzaker C, Hinshelwood RA, Peinado MA, Clark SJ. Epigenetic remodeling in colorectal cancer results in coordinate gene suppression across an entire chromosome band. *Nat Genet* 2006; 38:540-9; PMID:16642018; <http://dx.doi.org/10.1038/ng1781>.
17. Stransky N, Vallot C, Reyat F, Bernard-Pierrot I, de Medina SG, Segreaves R, et al. Regional copy number-independent deregulation of transcription in cancer. *Nat Genet* 2006; 38:1386-96; PMID:17099711; <http://dx.doi.org/10.1038/ng1923>.
18. Rauch T, Wang Z, Zhang X, Zhong X, Wu X, Lau SK, et al. Homeobox gene methylation in lung cancer studied by genome-wide analysis with a microarray-based methylated CpG island recovery assay. *Proc Natl Acad Sci U S A* 2007; 104:5527-32; PMID:17369352; <http://dx.doi.org/10.1073/pnas.0701059104>.
19. Novak P, Jensen T, Oshiro MM, Watts GS, Kim CJ, Futscher BW. Agglomerative epigenetic aberrations are a common event in human breast cancer. *Cancer Res* 2008; 68:8616-25; PMID:18922938; <http://dx.doi.org/10.1158/0008-5472.CAN-08-1419>.
20. Novak P, Jensen T, Oshiro MM, Wozniak RJ, Nouzova M, Watts GS, et al. Epigenetic inactivation of the HOXA gene cluster in breast cancer. *Cancer Res* 2006; 66:10664-70; PMID:17090521; <http://dx.doi.org/10.1158/0008-5472.CAN-06-2761>.
21. Clark SJ. Action at a distance: epigenetic silencing of large chromosomal regions in carcinogenesis. *Hum Mol Genet* 2007; 16(Spec No 1):R88-95; PMID:17613553; <http://dx.doi.org/10.1093/hmg/ddm051>.

22. Javierre BM, Rodriguez-Ubreva J, Al-Shahrour F, Corominas M, Graña O, Ciudad L, et al. Long-range epigenetic silencing associates with deregulation of Ikaros targets in colorectal cancer cells. *Mol Cancer Res* 2011; 9:1139-51; PMID:21737484; <http://dx.doi.org/10.1158/1541-7786.MCR-10-0515>.
23. Dallosso AR, Hancock AL, Szemes M, Moorwood K, Chilukamarri L, Tsai HH, et al. Frequent long-range epigenetic silencing of protocadherin gene clusters on chromosome 5q31 in Wilms' tumor. *PLoS Genet* 2009; 5:e1000745; PMID:19956686; <http://dx.doi.org/10.1371/journal.pgen.1000745>.
24. Dallosso AR, Oster B, Greenhough A, Thorsen K, Curry TJ, Owen C, et al. Long-range epigenetic silencing of chromosome 5q31 protocadherins is involved in early and late stages of colorectal tumorigenesis through modulation of oncogenic pathways. *Oncogene* 2012; PMID:22249255; <http://dx.doi.org/10.1038/onc.2011.609>.
25. Petzoldt JL, Leigh IM, Duffy PG, Sexton C, Masters JR. Immortalisation of human urothelial cells. *Urol Res* 1995; 23:377-80; PMID:8788275; <http://dx.doi.org/10.1007/BF00698738>.
26. Bello D, Webber MM, Kleinman HK, Wartinger DD, Rhim JS. Androgen responsive adult human prostatic epithelial cell lines immortalized by human papillomavirus 18. *Carcinogenesis* 1997; 18:1215-23; PMID:9214605; <http://dx.doi.org/10.1093/carcin/18.6.1215>.
27. Sommers SC, McManus RG. Multiple arsenical cancers of skin and internal organs. *Cancer* 1953; 6:347-59; PMID:13032927; [http://dx.doi.org/10.1002/1097-0142\(195303\)6:2<347::AID-CNCR2820060219>3.0.CO;2-L](http://dx.doi.org/10.1002/1097-0142(195303)6:2<347::AID-CNCR2820060219>3.0.CO;2-L).
28. Chen CJ, Chen CW, Wu MM, Kuo TL. Cancer potential in liver, lung, bladder and kidney due to ingested inorganic arsenic in drinking water. *Br J Cancer* 1992; 66:888-92; PMID:1419632; <http://dx.doi.org/10.1038/bjc.1992.380>.
29. Benbrahim-Tallaa L, Waalkes MP. Inorganic arsenic and human prostate cancer. *Environ Health Perspect* 2008; 116:158-64; PMID:18288312; <http://dx.doi.org/10.1289/ehp.10423>.
30. Straif K, Benbrahim-Tallaa L, Baan R, Grosse Y, Secretan B, El Ghissassi F, et al; WHO International Agency for Research on Cancer Monograph Working Group. A review of human carcinogens--part C: metals, arsenic, dusts, and fibres. *Lancet Oncol* 2009; 10:453-4; PMID:19418618; [http://dx.doi.org/10.1016/S1470-2045\(09\)70134-2](http://dx.doi.org/10.1016/S1470-2045(09)70134-2).
31. Wnek SM, Jensen TJ, Severson PL, Futscher BW, Gandolfi AJ. Monomethylarsonous acid produces irreversible events resulting in malignant transformation of a human bladder cell line following 12 weeks of low-level exposure. *Toxicol Sci* 2010; 116:44-57; PMID:20375083; <http://dx.doi.org/10.1093/toxsci/kfq106>.
32. Benbrahim-Tallaa L, Webber MM, Waalkes MP. Acquisition of androgen independence by human prostate epithelial cells during arsenic-induced malignant transformation. *Environ Health Perspect* 2005; 113:1134-9; PMID:16140617; <http://dx.doi.org/10.1289/ehp.7832>.
33. Jensen TJ, Wozniak RJ, Eblin KE, Wnek SM, Gandolfi AJ, Futscher BW. Epigenetic mediated transcriptional activation of WNT5A participates in arsenical-associated malignant transformation. *Toxicol Appl Pharmacol* 2009; 235:39-46; PMID:19061910; <http://dx.doi.org/10.1016/j.taap.2008.10.013>.
34. Jensen TJ, Novak P, Eblin KE, Gandolfi AJ, Futscher BW. Epigenetic remodeling during arsenical-induced malignant transformation. *Carcinogenesis* 2008; 29:1500-8; PMID:18448484; <http://dx.doi.org/10.1093/carcin/bgn102>.
35. Benbrahim-Tallaa L, Waterland RA, Styblo M, Achanzar WE, Webber MM, Waalkes MP. Molecular events associated with arsenic-induced malignant transformation of human prostatic epithelial cells: aberrant genomic DNA methylation and K-ras oncogene activation. *Toxicol Appl Pharmacol* 2005; 206:288-98; PMID:16039940; <http://dx.doi.org/10.1016/j.taap.2004.11.017>.
36. Hansen KD, Timp W, Bravo HC, Sabunciyan S, Langmead B, McDonald OG, et al. Increased methylation variation in epigenetic domains across cancer types. *Nat Genet* 2011; 43:768-75; PMID:21706001; <http://dx.doi.org/10.1038/ng.865>.
37. Behn-Krappa A, Hölker I, Sandaradura de Silva U, Doerfler W. Patterns of DNA methylation are indistinguishable in different individuals over a wide range of human DNA sequences. *Genomics* 1991; 11:1-7; PMID:1722485; [http://dx.doi.org/10.1016/0888-7543\(91\)90095-V](http://dx.doi.org/10.1016/0888-7543(91)90095-V).
38. Huschtscha LI, Noble JR, Neumann AA, Moy EL, Barry P, Melki JR, et al. Loss of p16INK4 expression by methylation is associated with lifespan extension of human mammary epithelial cells. *Cancer Res* 1998; 58:3508-12; PMID:9721850.
39. Tzeng CC, Liu HS, Li C, Jin YT, Chen RM, Yang WH, et al. Characterization of two urothelium cancer cell lines derived from a blackfoot disease endemic area in Taiwan. *Anticancer Res* 1996; 16(4A):1797-804; PMID:8712703.
40. Wu X, Rauch TA, Zhong X, Bennett WP, Latif F, Krex D, et al. CpG island hypermethylation in human astrocytomas. *Cancer Res* 2010; 70:2718-27; PMID:20233874; <http://dx.doi.org/10.1158/0008-5472.CAN-09-3631>.
41. Hawkins RD, Hon GC, Lee LK, Ngo Q, Lister R, Pelizzola M, et al. Distinct epigenomic landscapes of pluripotent and lineage-committed human cells. *Cell Stem Cell* 2010; 6:479-91; PMID:20452322; <http://dx.doi.org/10.1016/j.stem.2010.03.018>.
42. Ohm JE, McGarvey KM, Yu X, Cheng L, Schuebel KE, Cope L, et al. A stem cell-like chromatin pattern may predispose tumor suppressor genes to DNA hypermethylation and heritable silencing. *Nat Genet* 2007; 39:237-42; PMID:17211412; <http://dx.doi.org/10.1038/ng1972>.
43. Schlesinger Y, Straussman R, Keshet I, Farkash S, Hecht M, Zimmerman J, et al. Polycomb-mediated methylation on Lys27 of histone H3 pre-marks genes for de novo methylation in cancer. *Nat Genet* 2007; 39:232-6; PMID:17200670; <http://dx.doi.org/10.1038/ng1950>.
44. Epsztejn-Litman S, Feldman N, Abu-Remaih M, Shufaro Y, Gerson A, Ueda J, et al. De novo DNA methylation promoted by G9a prevents reprogramming of embryonically silenced genes. *Nat Struct Mol Biol* 2008; 15:1176-83; PMID:18953337; <http://dx.doi.org/10.1038/nsmb.1476>.
45. Lehnertz B, Ueda Y, Derijck AA, Braunschweig U, Perez-Burgos L, Kubicek S, et al. Suv39h-mediated histone H3 lysine 9 methylation directs DNA methylation to major satellite repeats at pericentric heterochromatin. *Curr Biol* 2003; 13:1192-200; PMID:12867029; [http://dx.doi.org/10.1016/S0960-9822\(03\)00432-9](http://dx.doi.org/10.1016/S0960-9822(03)00432-9).
46. Fuks F, Hurd PJ, Deplus R, Kouzarides T. The DNA methyltransferases associate with HP1 and the SUV39H1 histone methyltransferase. *Nucleic Acids Res* 2003; 31:2305-12; PMID:12711675; <http://dx.doi.org/10.1093/nar/gkg332>.
47. Coolen MW, Stirzaker C, Song JZ, Statham AL, Kassir Z, Moreno CS, et al. Consolidation of the cancer genome into domains of repressive chromatin by long-range epigenetic silencing (LRES) reduces transcriptional plasticity. *Nat Cell Biol* 2010; 12:235-46; PMID:20173741.
48. Reya T, Morrison SJ, Clarke MF, Weissman IL. Stem cells, cancer, and cancer stem cells. *Nature* 2001; 414:105-11; PMID:11689955; <http://dx.doi.org/10.1038/35102167>.
49. Edwards JR, O'Donnell AH, Rollins RA, Peckham HE, Lee C, Milekic MH, et al. Chromatin and sequence features that define the fine and gross structure of genomic methylation patterns. *Genome Res* 2010; 20:972-80; PMID:20488932; <http://dx.doi.org/10.1101/gr.101535.109>.
50. Cheng YT, Li YL, Wu JD, Long SB, Tzai TS, Tzeng CC, et al. Overexpression of MDM-2 mRNA and mutation of the p53 tumor suppressor gene in bladder carcinoma cell lines. *Mol Carcinog* 1995; 13:173-81; PMID:7619220; <http://dx.doi.org/10.1002/mc.2940130307>.
51. Webber MM, Quader ST, Kleinman HK, Bello-DeOcampo D, Storto PD, Bice G, et al. Human cell lines as an in vitro/in vivo model for prostate carcinogenesis and progression. *Prostate* 2001; 47:1-13; PMID:11304724; <http://dx.doi.org/10.1002/pros.1041>.
52. Weber M, Davies JJ, Wittig D, Oakeley EJ, Haase M, Lam WL, et al. Chromosome-wide and promoter-specific analyses identify sites of differential DNA methylation in normal and transformed human cells. *Nat Genet* 2005; 37:853-62; PMID:16007088; <http://dx.doi.org/10.1038/ng1598>.
53. Vrba L, Garbe JC, Stampfer MR, Futscher BW. Epigenetic regulation of normal human mammary cell type-specific miRNAs. *Genome Res* 2011; 21:2026-37; PMID:21873453; <http://dx.doi.org/10.1101/gr.123935.111>.
54. R_Development_Core_Team. R: A language and environment for statistical computing. 2010.
55. Rossi MR, Masters JR, Park S, Todd JH, Garrett SH, Sens MA, et al. The immortalized UROtsa cell line as a potential cell culture model of human urothelium. *Environ Health Perspect* 2001; 109:801-8; PMID:11564615; <http://dx.doi.org/10.1289/ehp.01109801>.
56. Bredfeldt TG, Jagadish B, Eblin KE, Mash EA, Gandolfi AJ. Monomethylarsonous acid induces transformation of human bladder cells. *Toxicol Appl Pharmacol* 2006; 216:69-79; PMID:16806342; <http://dx.doi.org/10.1016/j.taap.2006.04.011>.
57. Achanzar WE, Webber MM, Waalkes MP. Altered apoptotic gene expression and acquired apoptotic resistance in cadmium-transformed human prostate epithelial cells. *Prostate* 2002; 52:236-44; PMID:12111698; <http://dx.doi.org/10.1002/pros.10106>.
58. Horoszewicz JS, Leong SS, Kawinski E, Karr JP, Rosenthal H, Chu TM, et al. LNCaP model of human prostatic carcinoma. *Cancer Res* 1983; 43:1809-18; PMID:6831420.
59. Kaighn ME, Narayan KS, Ohnuki Y, Lechner JF, Jones LW. Establishment and characterization of a human prostatic carcinoma cell line (PC-3). *Invest Urol* 1979; 17:16-23; PMID:447482.
60. Stone KR, Mickey DD, Wunderli H, Mickey GH, Paulson DF. Isolation of a human prostate carcinoma cell line (DU 145). *Int J Cancer* 1978; 21:274-81; PMID:631930; <http://dx.doi.org/10.1002/ijc.2910210305>.